Low- Cost Magnetic Sensing System for Underground Mapping

Alon Shavit ID 302634423 Alon.Shavit@mail.huji.ac.il	Gal Zadock ID 200628998 Gal.Zadock@mail.huji.ac.il

Instructor:

Dr. Eyal Weiss,

Soreq Nuclear Research Center

Eyal_we@soreq.gov.il

September 2016

Table of Contents

Appendixes

Abstract

Magnetic mapping is an effective way to remotely locate underground objects made of iron or other ferromagnetic materials. It is usually done by moving a magnetic sensor over an area and measuring the magnetic magnitude at each point. Most of the existing mapping systems are very expensive because they are based on an atomic scalar magnetic sensor.

This work presents an innovative approach for reducing the price of magnetic mapping systems, by using a 3-axes vector flux-gate magnetic sensor. This sensor is inexpensive, but suffers from a critical problem of sensitivity to the natural earth magnetic field when it changes its orientation during the mapping process. This inaccuracy is formed mainly due to orthogonality imperfections between the sensor's axes that does not allow direct transforming of the three vector measurement axes to a scalar value. Hence, when the sensor rotates, a different magnetic magnitude is measured at each orientation. Therefore, it was currently impossible to use this kind of sensor for mapping purposes, without any calibration procedure.

We developed a comprehensive physical model which simulates the entire problem. By using its results, we developed an efficient calibration technique, which solves this problem by applying a correction transformation on the sensor's raw data. The calibration is made by manually spinning the sensor over random orientations. The gathered magnetic data is then used as an input for a calibration algorithm, which is based on ellipsoid fit by RMS. The algorithm's output is a calibration matrix and an offset vector. By applying those correction parameters on a sensor's raw data, it can accurately measure magnitude at all orientations. In addition, we found the recommended hardware configuration to be used with this calibration algorithm to insure minimum calibration errors.

The system was tested in many experiments, which showed a significant reduction of error parameters in a calibrated sensor. The mean magnitude max peak to peak (PTP) error reached <15 [nT] for a sensor's rotating at different orientations, while the mean magnitude variance reached <3 [nT]. These results are much better than 652[nT] and 24,055 [nT], respectively, for the same sensor without calibration.

In order to demonstrate the calibrated sensor's mapping capabilities, we developed a mapping algorithm and a mapping method, which enable using the calibrated sensor to create a magnetic map of a given area. This map shows the relative magnetic magnitude at a given coordinate, according to the sensor's location. The map enables detection of magnetic anomalies which are caused by the existence of ferromagnetic materials. In addition, we developed a friendly graphical user interface, which makes the calibration and the mapping process very fast and intuitive.

Introduction

Ferromagnetic materials affect the magnetic field lines, creating a magnetic field anomaly in their area[1]. This anomaly can be detected by measuring the magnetic field's strength at different sampling points located inside a given area of interest. Then, by looking for magnetic anomalies in the domain, the location of the ferromagnetic materials can be estimated[2]. Magnetic mapping has many possible applications. Researchers suggest using this technique to detect heavy metals[3], archeological and prehistoric tools[4], underground pipes[5], and even airplanes' sunken parts[6].

There are some methods to define the resolution of the measurement. In this work we used two parameters to model a measurement's errors. The first parameter is the difference between the highest to the lowest magnetic magnitude, max peak to peak error (PTP error). The second parameter is the magnitude variance. Both parameters are calculated from the measured data during a given measurement scenario. Figure 1 shows the PTP error parameter for a given set of data:

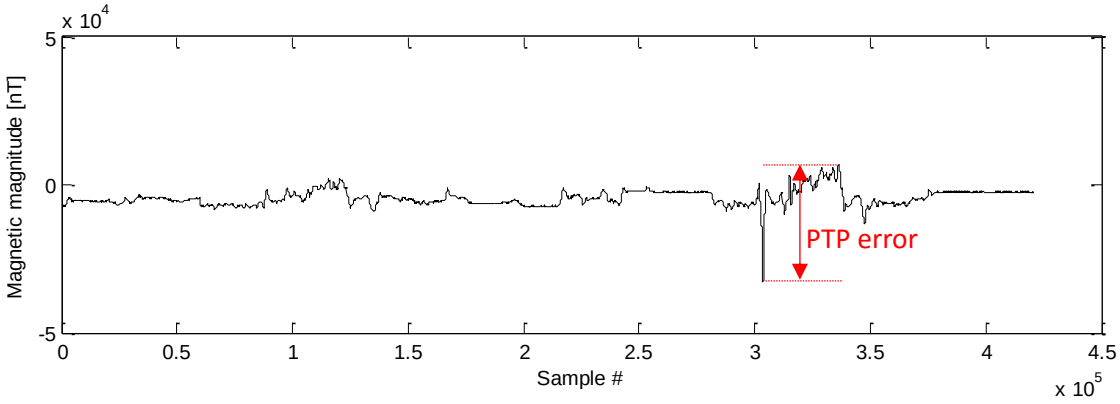

***Figure 1 – An illustration of the PTP error parameter**. The magnetic magnitude as a function of the sample's index*

In order to detect a magnetic anomaly, the instrument which is used for measuring the magnetic data must have a **lower** magnitude error compared to the typical change created by the existence of the ferromagnetic material. Otherwise, the uncertainty of the magnitude's value might be higher than the signal produced by the magnetic anomaly. Different applications require different magnitude sensitivities. Figure 2 presents the typical sensitivity that is required for some common magnetic applications[7]:

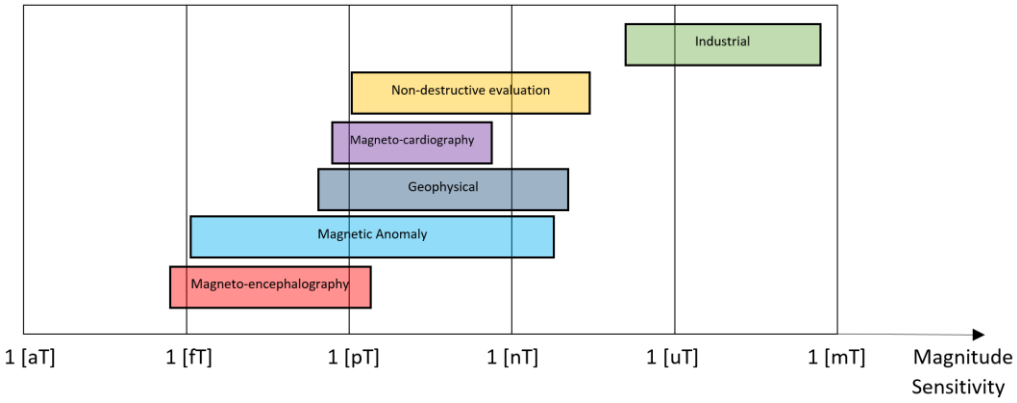

Figure 2 – Required magnetic magnitude sensitivity for some applications

In this paper we focused on creating a capability of magnetic anomaly mapping. Therefore, the magnitude sensitivity must be in the order of ~10 [nT] or lower in order to enable magnetic anomaly measurements.

The mapping is usually done by moving a sensor over an area, while measuring the scalar field strength as a function of the sensor's location in space. In this work, we focused on the simplest possible scanning configuration, in which the scanning process is done manually by walking over the area. Therefore, the sensor is being held by hand during all the mapping process. Hence, while mapping an area, the sensor might change its orientation (for example, clockwise or counter clockwise).

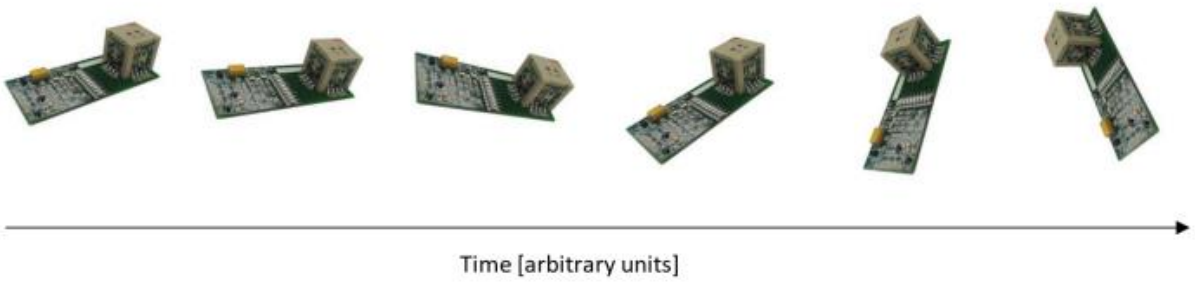

***Figure 3 – An illustration of possible orientations of the sensor during scanning**, as a function of time*

The simplest way to conduct a magnetic mapping is by using scalar magnetic sensors[8] , such as Geometrics' G-823A cesium magnetometer[9]. These types of sensors have a maximum magnitude difference (PTP) of about 0.3 [nT] over 360 degrees rotation[10], which makes them suitable for

magnetic mapping purposes. However, a scalar sensor suffers from "dead zones" in some sensor orientations and is a very expensive instrument, having a tag price of about 50k$.[11]

Another alternative is using a fluxgate sensor. This is a low- priced (~ 500k$ for some models[12]) vector sensor, which its output consists of the magnetic field x-y-z components. The sensor we used in our work is a 3 axes fluxgate sensor and is made of 3 pairs of sense and drive windings[13]. In order to correctly measure the magnetic vector component at each x/y/z direction, all the windings pairs have to be placed perfectly perpendicular upon each other. It creates an orthogonal system, which allows calculating the total magnetic magnitude by using the formula $|B| = \sqrt{{B_X}^2 + {B_Y}^2 + {B_Z}^2}$.

However, due to mechanical imperfections, the windings are not perfectly perpendicular to each other. Therefore, a non- orthogonal coordinate system is formed (with axes W_1, W_2 and W_3). The non-orthogonality errors between the axes can be modeled by three angles, v_{12}, v_{23} and v_{13} , which represent the angular deviation from an orthogonal system (with axes u_1, u_2 and u_3)[16].

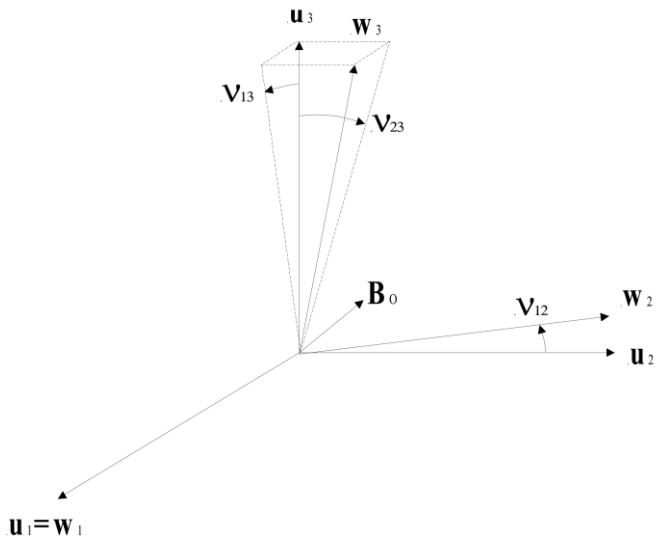

Figure 4 – The different coordinate systems of a fluxgate magnetometer[16]. *the orthogonal system is defined by the axes u1, u2 and u3, while the non-orthogonal system is defined by the axes W_1, W_2 and W_3. The orthogonality errors are modeled by the angles, v_{12}, v_{23} and v_{13}*

In addition, fluxgate magnetic sensors suffer from a constant magnetic offset, formed by a constant magnetic field. This constant field is formed by ferromagnetic materials and electrical currents which are emitted from the sensor unit itself[14].

These imperfections lead to very significant magnitude errors when the sensor spins in 360 degrees (max PTP of ~650 [nT] and variance of ~24000[nT]). Therefore, it is impossible to use the fluxgate sensor for our purposes, without overcome those problems.

There are some different approaches regarding how the calibration problem should be handled. Because the value of all v_{ij} (i={1,2}, j={2,3}) are small ($v_{ij} \sim 1^{o}$), most of the calibration methods use small angle approximation. Because it is a linear problem, most of the methods are based on applying a linear transformation over the raw sensor data[14]. The fundamental difference between the different approaches is the method which is used in order to find the calibration parameters. Those parameters are unique to a given fluxgate sensor, and may even change during time due to mechanical and temperature variations[15].

One approach for estimating the calibration parameters is using a scalar reference magnetometer[16]. Mathematical solutions were proposed by research groups working on calibration of satellites' magnetometers during magnetic mapping missions[17]. The proposed solutions are based on the assumption that the intensity of the magnetic field where the magnetometer is rotated is precisely known. Another solutions, aimed for spacecraft equipped with a fluxgate sensor, use a scalar reference to enable real time calibration during typical spacecraft mission mode operations[18]. The reported magnetic magnitude variance of the scalar calibration is about 2-4 [nT][19]. However, all those methods use an expensive scalar magnetometer, while forcing the user to use an external device. Therefore, we found those techniques unsuitable for our needs.

Other methods suggest a calibration which is based on moving the sensor inside a constant (unknown) magnetic field. This is called vector calibration because the output of the vector magnetometer is compared with the total magnetic field strength[20]. A full theoretical model which generalizes the problem has been suggested, and proved that the determination of all calibration parameters from a motion inside a constant magnetic field is possible[21].

The geometric approach calibration is a vector calibration technique which was presented in several articles. This technique is capable of dealing with a constant field offset and non-orthogonality problems. The calibration is done by finding an estimator which yields the calibration parameters, which produce the best geometric fit to the sensor readings. This technique does not require any external reference[22]. Some calibration algorithms which are based on a geometric approach have been published[23], and some were even demonstrated very recently in some applications like calibrating a compass mechanism of underwater gliders [24]. The geometric approach which we used

in our work is called Ellipsoid fitting. This calibration alternative, which was suggested in some articles[25,26,27], will be discussed during the methods part of this paper.

However, most of the reviewed articles focused on the theoretical aspect of the calibration algorithm, and those which presented a possible application have focused on applying an algorithm on a very specific given system configuration.

Therefore, in this paper we chose to focus on the **system engineering** aspect of building a complete mapping system for underground magnetic mapping. Hence, this work has examined the influence of each independent sub-system on the final system's performance. The research was made by considering all the separate aspects which are required to create a fully functional system, based on the "System of Systems" design concept[28]. It involved characterization of all the components which are necessary for the creation of a functional mapping system.

In order to profoundly understand the different parameters which affect the final system's errors, a comprehensive physical model must be developed. This model should consider all the physical, algorithmic and hardware properties of the system.

Hence, our goal is to find the essential design rules and the main system tradeoffs, to be used by engineers who develop magnetic mapping systems. There are three main sub-systems in our design: the hardware system, the calibration algorithmic system and the mapping system. Each of those sub systems is being analyzed in this paper to find its most suitable configuration for the final mapping system. As a result, the main goals of this project are (1) developing a calibration technique which creates a sensor with magnitude sensitivity of ~10 [nT] or lower, (2) finding the most suitable hardware configuration while modeling the effect of relevant parameters on the final system performance and (3) creating a mapping method which is meant to be used with a calibrated sensor for the creation of a visual map of magnetic anomalies in a given area.

Materials and Methods

Solution Overview

Our solution is based on a linear transformation, which is applied on the sensor's raw data. This transformation solves the problem of the non-orthogonal axes by converting each x-y-z data sample (which represents the vector components of the magnetic field at a given time) into a new, corrected data. The new data is almost similar to the data which would be measured by a perfectly orthogonal sensor. In order to create this transformation, we developed a comprehensive calibration method. By creating an advanced simulation environment, we found a suitable hardware configuration for this process. As a result, calibrated magnetic data can now be transferred to our unique mapping algorithm, which creates a visual magnetic map of an area.

Figure 5 presents a block diagram which demonstrates the data flow in our solution:

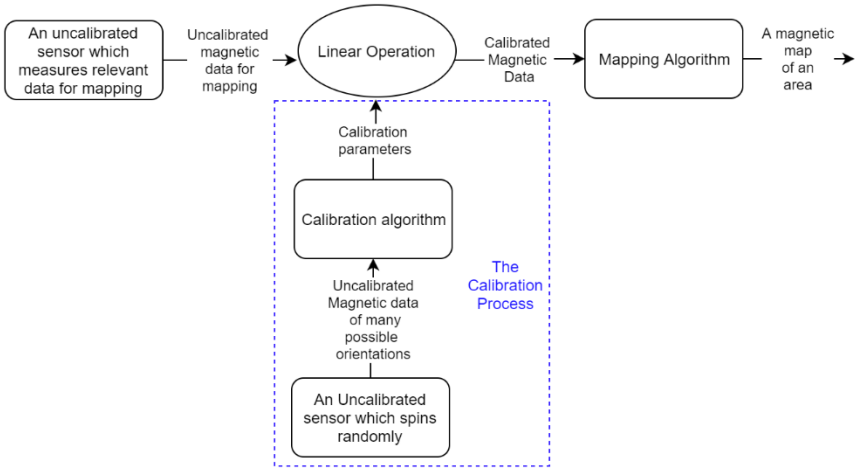

Figure 5 - The system's data flow

Methods

Calibration method

Calibration means relating the output of a magnetometer to the value of the external field[21]. In our work the reference external field is the earth's natural magnetic field (~45,000[nT] in Israel). An ideal scalar magnetometer, which measures a constant magnetic field would show a constant magnitude irrespective of the magnetometer's orientation. Therefore, each data measurement point has the same distance from the origin ($|B| = \sqrt{{B_X}^2 + {B_Y}^2 + {B_Z}^2} = Const$). Hence, when plotting the magnetic data of different sensor's orientations, a perfect sphere is formed.

However, as explained previously, a fluxgate magnetometer suffers from non-orthogonality between its axes. Therefore, measurement anomalies are obtained in respect to the magnetometer's orientation.

Readings of a non-ideal sensor always lie on an ellipsoid manifold[23]. Therefore, by using a linear transformation, it is possible to recast the calibration problem into a unified transformation parameterized by: rotation **(R)**, scaling **(S)** and offset **(b)**. This approach creates a linear problem that may be solved by using known linear methods[22].

The rotation and scaling are due to the non-orthogonality between the axes, while the offset (the ellipsoid's displacement from the origin) is due to constant ferromagnetic disturbances formed by the magnetometer itself. The solution for this problem is done by using an algorithm which performs a linear transformation of the magnetometer's readings. The algorithm fits all the points into an ellipsoid manifold, which is centered in the origin. After applying the transformation, all the data measurement points (among the magnetic readings) have the same distance from the origin. Since this distance is defined by $\sqrt{{B_X}^2 + {B_Y}^2 + {B_Z}^2}$, the result is a constant magnetic magnitude, irrespective of the sensor's orientation.

There are several approaches regarding how to transform an ellipsoid into a sphere[29] while minimizing the fitting error. The algorithm which was used in this work is "Ellipsoid fit" by Petrov Yuri[30]. This algorithm returns the algebraic description of the ellipsoid by nine parameters: semi-axis (a, b, c), Euler angles (φ, θ, Ψ) (repressing the successive axis rotations) and coordinates of the center (X_0, Y_0 , Z_0). This representation of the ellipsoid also called the quadratic form (by nine coefficients). In addition, the algorithm also returns the geometric description: center, radii and principal axes. The fitting is done by performing a linear convex optimization on the raw data $\boldsymbol{h_r}$ to minimize the error of the fit, by minimizing the sum of squared algebraic error distances (RMS).

According to those returned values, the correction matrix **(M)** and the offset vector **(b)**, which best transform the ellipsoid into a sphere, which is centered in the origin, are calculated. **M** is calculated by using R' (de-rotation) and $\boldsymbol{S^{-1}}$ (de-scaling). The corrected data ($\boldsymbol{h_c}$) is then given by using the formula below:

$$h_c = M(h_r - b); (s.t\ M = S^{-1}R')$$

To supply the input data for the algorithm, a constant magnetic field has to be used during all time of calibration. For this purpose, the earth's magnetic field, which can be considered as a strong and constant field, was used.

In order to collect calibration data, the sensor is rotated by hand for a long period of time (~5 minutes). The data which has been collected during this process is used as an input for the correction algorithm. The algorithm's output is a correction matrix and an offset, which are individual for each magnetometer. After applying the matrix and the offset on the sensor's raw data, we get improved data which is much closer to the data of an ideal sensor.

Figure 6 demonstrates the calibration process:

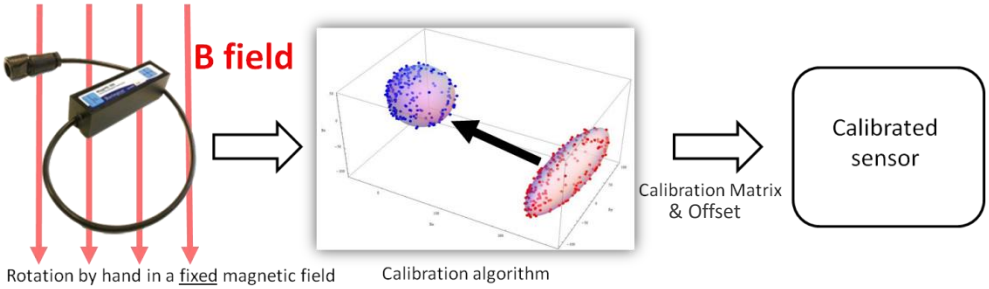

Figure 6 - The calibration process data flow

Method for finding the best hardware configuration

The performance of the described calibration algorithm is affected by the chosen hardware configuration and the properties of the calibration process (speed and duration of spinning, sampling rate, etc.). Therefore, a very significant part of the system's design was the creation of a simulation environment. The created simulation enables virtual testing of many possible hardware setups, without the need of physically building one. Many sessions of simulation were conducted to find the hardware properties which most affect the error parameters. Then, the hardware configuration was changed according to the conclusions. The simulation considers all the physical and algorithmic properties of the system and the calibration process. Some simulation examples can be seen on Appendix 2.

The simulation works by choosing r random points in a 3D sphere. Each point represents a different rotation direction of the sensor. Then, an interpolated path is created (by creating linearly- spaced new points) between each 2 random points. The sensor's x-y-z analog data is simulated by using the values below:

- Orthogonality error between axes: 1 degree. This is the maximum orthogonality error according the sensor's specification[1].
- External magnitude: 45k nT (this is an approximation for the strength of the earth's magnetic field[31]).
- "Analog sampling" rate: 50kHz.
- Build- in sensor's low pass filter. In order to simulate the sensor's filter, we created an IIR low pass filter[32] with a controlled bandwidth. The filter was designed to achieve a -3dB reduction of the signal at the maximum bandwidth. The bandwidth value was changed according to the sensor module which has been simulated.

white noise and pink noise are added to the "analog signal" by using max self-noise of 0.1 [nT] and alpha parameter (for the pink noise) of -0.75 (this is a good approximation of the $1/f^{\alpha}$ noise[33])

Then, each axis is sampled with a digital frequency *f*, while simulating sampling imperfections. Those imperfections are added to the system by using unwanted averaging every 5 samples. This was done in order to module a real A/D sampler, which does not sample the data in zero time. The raw magnetic magnitude and the maximum PTP value are then calculated using this data. Finally, the calibration algorithm is applied on the data, and the corrected magnetic magnitude and the new maximum PTP value are recalculated.

Mapping algorithm

Magnetic mapping is a common way to track ferromagnetic martials. The mapping is usually done by a crossing of a measurement instrument within the area. After calibrating a sensor, we wanted to enable the user to create a magnetic mapping of an area. Therefore, we developed a unique algorithm, which converts calibrated magnetic data into a visual, colored map of the area of interest. The algorithm assumes that the area is divided into ***n*** scanning strips, with a distance ***d*** between each 2 adjoining strips (***d*** is the scanning resolution). Another assumption is a constant speed of scanning, denoted by ***v***. The Scanning process is done in the steps below:

1. Place the calibrated sensor at the beginning of the first strip, with its edge heading left (scanning orientation).

[1] Appendix 1 –*Specifications*

2. Walk with the sensor in a constant velocity v, without changing the sensor's heading.
3. When reaching the end of the strip, **change** the sensor's heading, so it is heading right (idle orientation) instead of left (scanning orientation).
4. Move the sensor to the beginning of the next strip, while keeping its heading to the right.
5. When reaching the beginning of the next strip, change the sensor's heading to the left and repeat stages 2-5.
6. When the scanning is terminated, change the sensor's heading to the right.

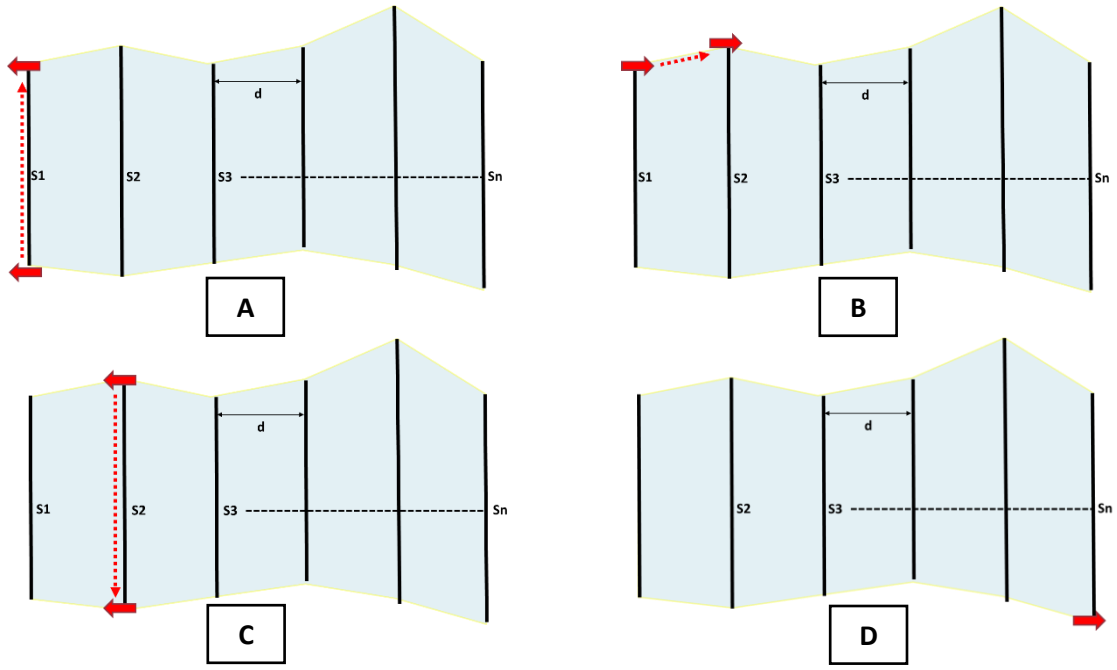

Figure 7 – Scanning process*. The sensor's heading is demonstrated using a red arrow. A: Scanning the first strip. B: Moving from the first strip to the second strip. C: Scanning the second strip. D: heading when scanning is terminated.*

While scanning the area using the described process, the magnetic field data is saved on the computer using a Labview application. The data consists of a very large number of calibrated x-y-z points- each one represents the magnetic field vector components in a given time during the scanning.

The points are then transferred into our mapping algorithm. This algorithm works as described below:

- Input:
  a. Q – group of p>1 points. Each point has its own magnetic x-y-z coordinates.
  b. v – Velocity of scanning [meter/sec].

c. d – Scanning resolution [m].

d. f – Sampling frequency [1/sec].

- Output:
  a. A matrix **M** with dimensions k x 3, where k is the total number of points which were measured when the sensor was in the **scanning orientation.** For a given point which has the index i ($1 \leq i \leq k$):
     - M(i,1) represents the x coordinate of the point
     - M(i,2) represents the y coordinate of the point
     - M(i,3) represents the magnetic magnitude deviation from the average at the x-y location [M(i,1), M(i,2)].

- Way of operation:

  The algorithm extracts the data which was created during the sensor was in a scanning orientation. Then, by biasing the measurements in respect to the mean magnitude's value, magnetic anomalies can be obtained. The data is then plotted to create a colored magnetic map of the area. The detailed way of operation given below:

  a. Find the minimum and maximum magnetic value for each axis (x, y and z), among all the points in goup Q.
  b. The axis with the largest value of Abs(min – max) is defined as the "strongest axis". The assumption here is that by finding the axis which has the maximum value of change during the scanning, we could differentiate between the 2 possible orientations of the sensor (scanning and idle). It can be done by assuming that the earth has a strong and constant vector magnetic field.
  c. For a given x-y-z point, if the strongest axis has a value of 0.6*abs(max) or above, define this point as a part of the "scanning orientation" group (S). Otherwise, define this point as a part of "idle orientation" group (I).
  d. Define a group G, consists of n subgroups. Each subgroup consists of points $\in S$, which are bounded between at least 10 points $\in I$.
  e. For each $g_i \in G$, $1 \leq i \leq n$, calculate its length l_i (in meters) by: $l_i = (|g_i| - 1) * \frac{1}{f} * v$.
  f. Create a matrix M of size $[|S| \; x \; 3]$. Set all the values to 0. The first column represents the x coordinate, the second column represents the y coordinate

and the third column represents the magnetic deviation from the average for the given x-y location [M(i,1), M(i,2)].

g. Calculate $|\bar{g}|$ - the averaged value of all the magnetic magnitudes of points $g_i \in G$, $1 \leq i \leq n$.

h. For each group of points g_m $(1 \leq m \leq n)$. Set the matrix M to be $(1 \leq j \leq |g_m|)$:

- M(j,1) = d*(m-1) (note that the x coordinate of the first strip is 0).
- $M(j,2) = \begin{cases} l_m * \left(\frac{j}{|g_m|}\right), & , m = 1 \\ M(|g_{m-1}|, 2) + l_m * \left(\frac{j}{|g_m|}\right), & j \neq 1, m \text{ is odd} \\ M(|g_{m-1}|, 2) - l_m * \left(\frac{j}{|g_m|}\right), & m \text{ is even} \end{cases}$
- M(j,3) = $Abs[\sqrt{g_{1jx}{}^2 + g_{1jy}{}^2 + g_{1jz}{}^2} - |\bar{g}|]$, when g_{jkl} stands for coordinate l ($l \in \{x,y,z\}$) in the k[th] point of group g_j. This is the magnetic deviation from the average, when the sensor in on scanning orientation.

A graphical demonstration of the mapping algorithm is shown in Figure 8:

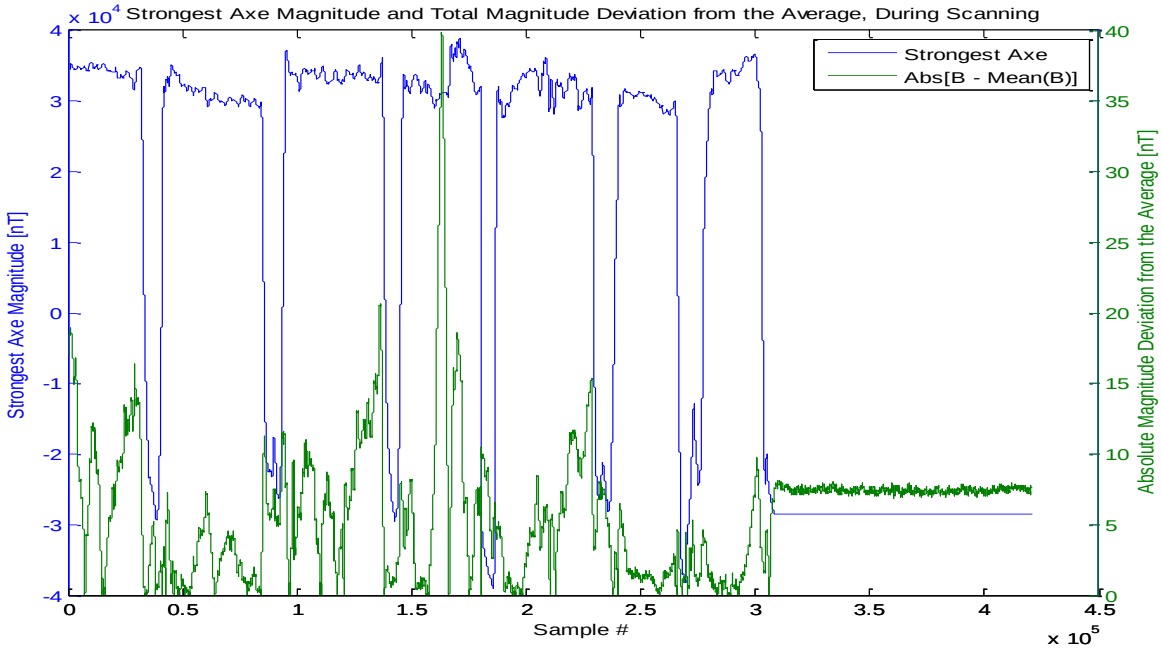

Figure 8 – A graphical example of the mapping algorithm*. The blue graph shows the strongest axe, while the green graph shows the absolute magnetic deviation from the average during scanning. The peak in the green graph is created when the sensor passes above a Ferromagnetic material*

A colored map, which represents the relative magnetic magnitude in x-y coordinates system, is produced out of the matrix M, by using Matlab's function "linespace"[34]. The Matlab code produces a linear interpolation, so it is possible to estimate the magnetic field between the scanned strips. As we show in the result session, this approach was found to be suitable for creating reliable magnetic mapping of an area.

Testing Methods

Primary Tests

An important goal of this project was to understand the different hardware considerations which affect the final system's errors. Therefore, after designing a primary solution, by using the simulation, we had to check the correctness of our analysis. Since the system consists of many dependent components, we decided to conduct several controlled field experiments in order to make sure our analysis regarding the optimal solution was correct. In each experiment, the sensor was rotated by hand for a known period of time. The person who rotated the sensor had no ferromagnetic materials on his body. This process was repeated several times to get reliable results. After each experiment, the data was analyzed by our Matlab software. All the measurements took place in a "clean area", where the magnetic noise is relatively low.

Two different models of sensors were tested. The main difference between the two is the 3dB band width. While the first model (Bartington Mag 648) has a BW of 30Hz, the second model has a BW of 1kHz.

In addition, some systems use an internal averaging mechanism, which calculate an averaging of several measurements in the hardware. In this kind of systems, the output data, which is transferred to the algorithm is actually averaged data of several measurements.

The controlled parameters were:

- Speed of rotation during the calibration process - some different speeds were tested qualitatively.
- Rotation time- some different times were tested.
- Sensor model and BW – Mag 648 compared to Mag 649.
- Internal averaging– a system with and without internal averaging.

The measured parameters were:

- Ellipsoid Fitting algorithm– 2 possible fitting algorithms were checked. The first one is performing the fitting using RMS (root mean square) calculation[30], while the second one is trying to fit an ellipsoid to a sphere with the same volume[35].
- Max magnitude PTP (peak to peak) error - the max PTP within the magnetic magnitude (units of [nT]). We want this parameter to be as small as possible.
- Magnitude's variance – the variance of the magnetic magnitude (units of [nT]). We want this parameter to be as small as possible.

Final Configuration Tests

After we tested some optional hardware configurations and calibration properties, we decided to focus on cases where the sensor's angular velocity is relatively low (compared to its BW). Therefore, the final configuration tests included cases where the sensor rotates relatively slowly. All the measurements took place in a "clean area", where the magnetic noise is relatively low. We had 4 hardware configurations. In each hardware configuration, several measurements were made. Each measurement lasted for 60 seconds. During this time, the sensor was manually spinning at random directions.

The different hardware configurations are shown below:

Hardware configuration #	Magnetic sensor model	Sampling rate
1	Bartington Mag649	250Hz
2	Bartington Mag649	3000Hz
3	Bartington Mag648	250Hz
4	Bartington Mag648	1000Hz

Table 1 – Possible hardware configurations of the final system

Tests to distinguish between different approaches for calculating the correction matrix

As we show in the 'Results' section of this paper, the final configuration's tests showed a major improvement in the error indicators (max amplitude PTP and magnitude variance). Therefore, we wanted to test different approaches for calculating the correction matrix. As we explained in the introduction, we want to understand which of the parameters has the most effect on the performance parameters of the system.

There are different approaches regarding how to collect data for the calibration process. As we explained before, each sensor rotation lasts for about 60 seconds, and it is considered as "one

measurement". When calibrating the sensor, several measurements are made. We can relate to each one of the measurements, as a single attempt for a scalar magnetic mapping.

As in real life, we do not know the exact way the user would move the sensor (exact orientation, exact speed, etc.). Therefore, our challenge is to calibrate the system in a way which would lead to the lowest mean errors possible in a given unknown measurement. In other words, the calibration procedure should be done once, while the calibrated system should be best fitted to all the possible orientations the sensor may have during an operation.

In this experimental session we related to each single measurement in a given hardware configuration as a module to a possible way of operation, as we just described. The calibration matrix is made out of the raw data we got from the experiments in each hardware configuration. We have three different alternatives of choosing the data which would create the calibration matrix, which are summarized in Figure 9:

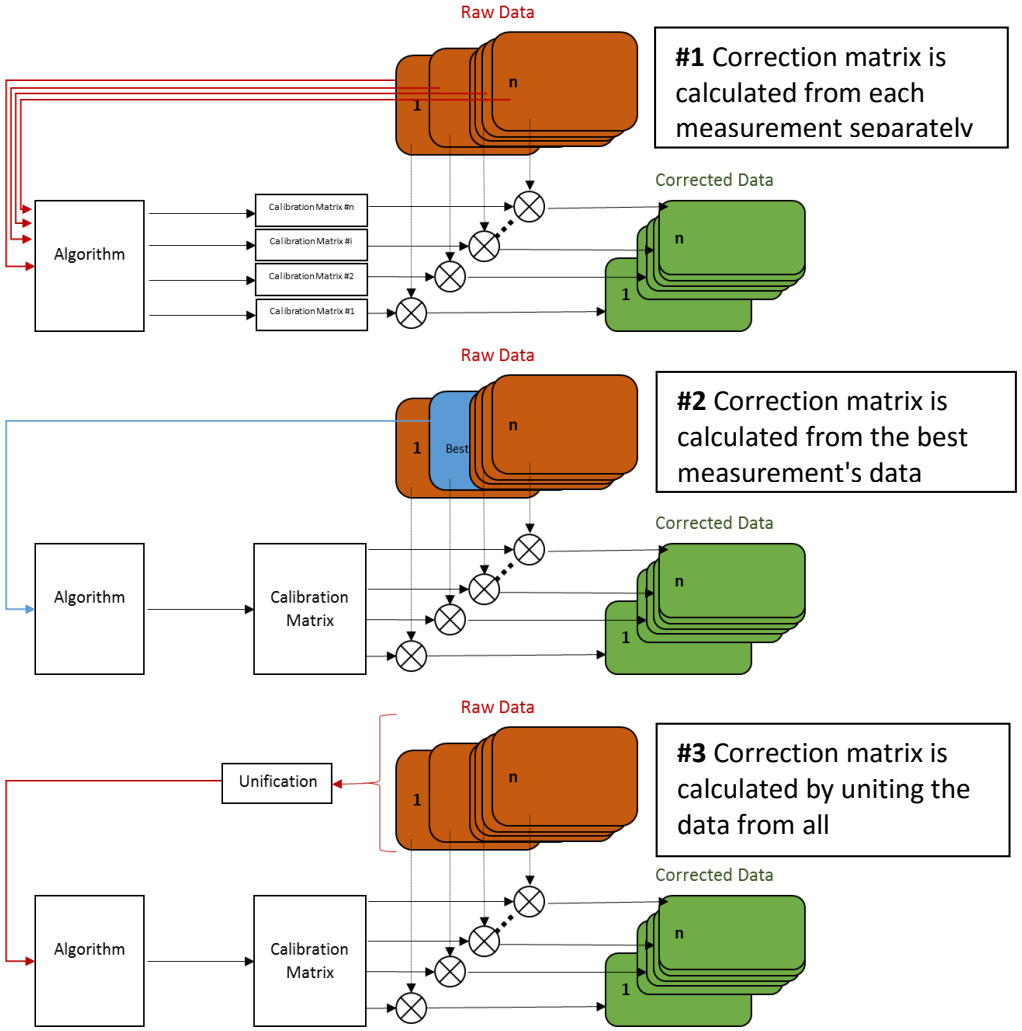

Figure 9- Different approaches for creating the correction matrix

In alternative #1, the corrected data is calculated exclusively for each set of raw data. Therefore, we get several calibration matrixes – one matrix per data set. In alternative #2, the data set which yields the best error parameters is selected and its calibration matrix is used over all the other sets. In alternative #3, we unite all the raw data from all the separate sets, so that we get a very long set of data ("united data"). Then, we use the calibration algorithm on this long set in order to get the calibration matrix. This calibration matrix is then used for the correction of all sets.

Averaging considerations

During the analysis we found that if we apply a moving average filter on the magnitude signal, it could improve the errors. In order to choose the appropriate window width of the filter, we had to consider the characteristics of our target; Let us assume that our smallest target is about 1-meter width. Therefore, we want the mapping resolution to be twice better. **Hence, mapping resolution = 0.5 [m].** After calibration, the mapping process will be done by slowly walking over the target area. Since a human's walking speed is about ~1 [m/sec], the smallest resolution would be mapped in a period of time of about 0.5[m]/1[m/sec] = 0.5[sec]. Therefore, the widest theoretical possible moving average window is 0.5[sec].

We wanted to compare two possible window widths – 0.5 sec and 0.25 sec. If the differences between those two wouldn't be so dramatic, we prefer to choose the 0.25 sec window in order to get a better mapping resolution and a faster possible scanning speed. In order to test it, we decided to compare the two possible windows in the Mag649 sensor with sampling rate of 250Hz. The high sensor BW, combined with the relatively low sampling rate helps to create a module which is also relevant for the rest of the hardware configurations.

Mapping Tests

After creating the mapping matrix, using our mapping algorithm, several mapping tests were made. Those tests demonstrate the final performance of our system. As we explained in the introduction, our entire project was aimed to enable magnetic mapping by using low cost hardware. Therefore, the mapping tests are the ultimate approach to test our system functionality in "real life". The tests were taking place in a clear area. They were made by placing a ferromagnetic object (screwdriver or a laptop) within the area of interest. Then, the mapping process was performed, as described in the mapping algorithm session.

Materials

Hardware Configuration

To transform to sensor's analog signal into digital data which can be analyzed by a computer, a 24-bit sampler was used. Earth magnetic field PTP is ~90k [nT]. When using a standard 16 bit sampler, the sampling resolution is $\frac{90000}{2^{16}} = 1.3[\text{nT}]$. For minimal sampling errors we wanted the sampling resolution to be less than 1[nT]. Hence, when using the 24 bit sampler, we achieve a resolution of $\frac{90000}{2^{24}} = 0.005[\text{nT}]$. The sampled signal is then transferred into the computer. The hardware components we used are presented in Figure 10:

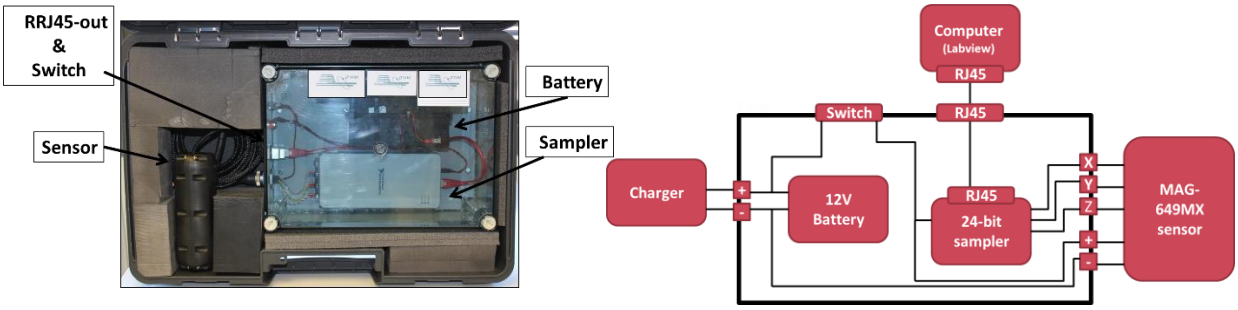

***Figure 10- Final hardware configuration**. A- An overall picture , B- The Hardware's Scheme*

The system consists of the main components which are described in Table 2:

Index	Component name	Model	Comments
1	Sensor	Bartington Mag 648 / Mag 649	
2	1-Slot sampler chassis	NI cDAQ-9181	24-bit sampler.
3	Sampler	NI 9139	Sampling rate of 50kHz in order to reduce the noise per Hz, by spreading the total noise over wide BW.
4	Rechargeable battery + charging connector	Vision CP12120	
5	Internal Ethernet cable	Standard RJ45 cable	
6	External Ethernet cable	Standard RJ45 cable	
7	Laptop		
8	Data Cables sensor to sampler		3 differential signals

9	Switch	Standard on/off switch	

Table 2 – A List of components of the final system's configuration

Labview Application

The sampler NI-9239 was connected to the computer through an Ethernet cable. In the computer we used a Labview based application in order to collect the data and to create the data files, which are analyzed by the Matlab software.

Matlab Based Software

We used Matlab for the implementation of the simulation environment. In addition, matlab was used for implementation of the calibration algorithm. Furthermore, we created a Matlab based friendly graphical user interface, which implements both the calibration algorithm and the mapping algorithm.

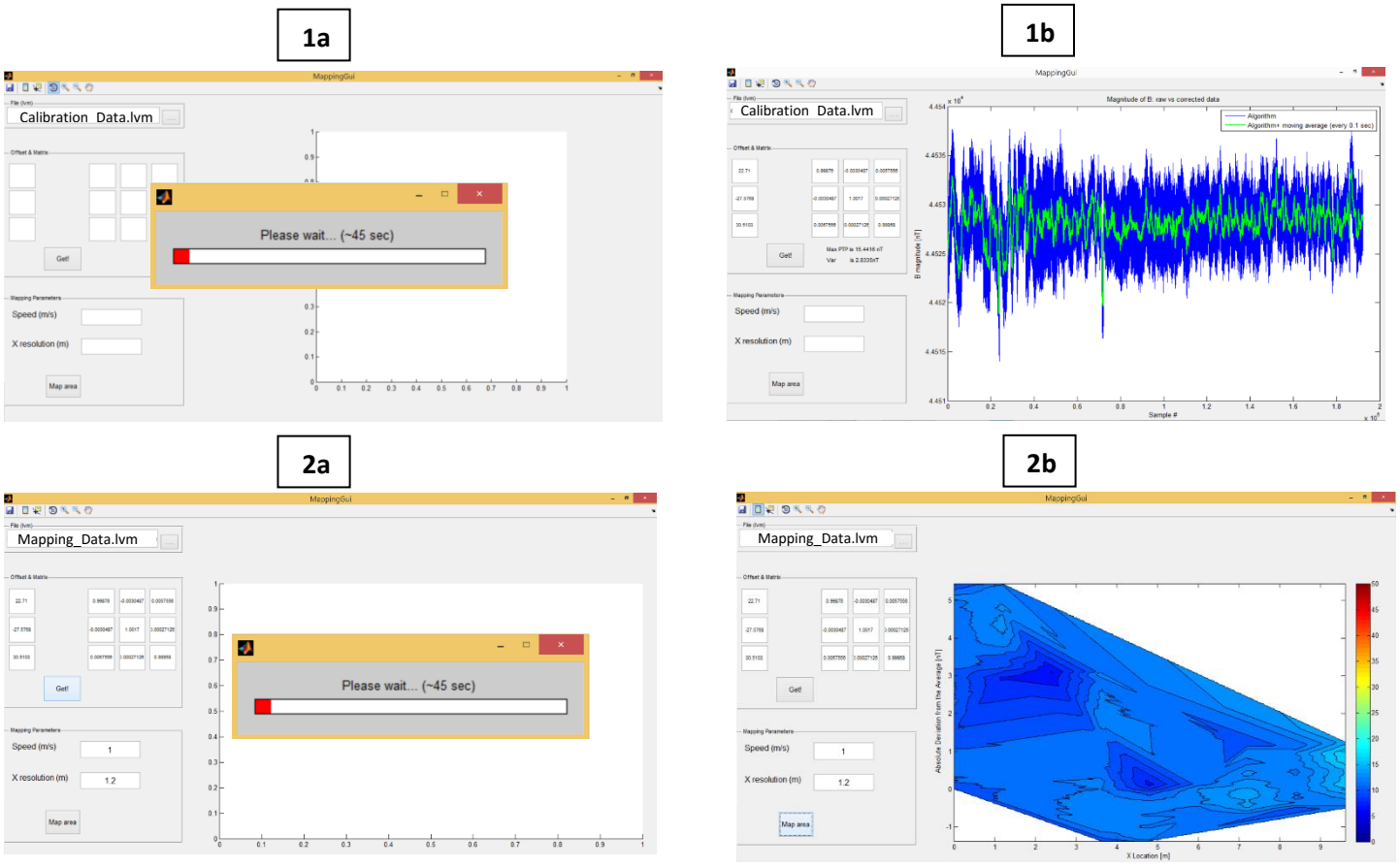

Figure 11 - Matlab based GUI. *1: Applying the calibration algorithm on a data file (a) to get the calibration parameters (b)*
2: Applying the mapping algorithm on a data file (a) to get a magnetic map of the area (b)

Results

Affecting parameters

Fitting Strategy

In all the experiments, the ellipsoid fit algorithm which is based on fitting by RMS, has shown better error rates (magnitude's variance and max PTP) compared to the algorithm which is based on fitting by volume. The performance was 15%-40% better in all the experiments.

Speed of rotation and internal averaging

For a system with an internal averaging mechanism (every 5 samples) the errors were very significant. The results can be seen in Table 3:

Speed of rotation/ calibration performance	PTP		Variance	
	Raw data	Corrected data	Raw data	Corrected data
Slow rotation	1116	676	29,585	4,633
Fast rotation	5010	4,721	374,873	335,100

Table 3 – Averaged results of experiments with a system which has internal averaging *for slow speed of rotation and fast speed of rotation*

Moreover, the calibration results were affected from the speed of rotation. An example of the influence of this parameter can be seen in Figure 12.

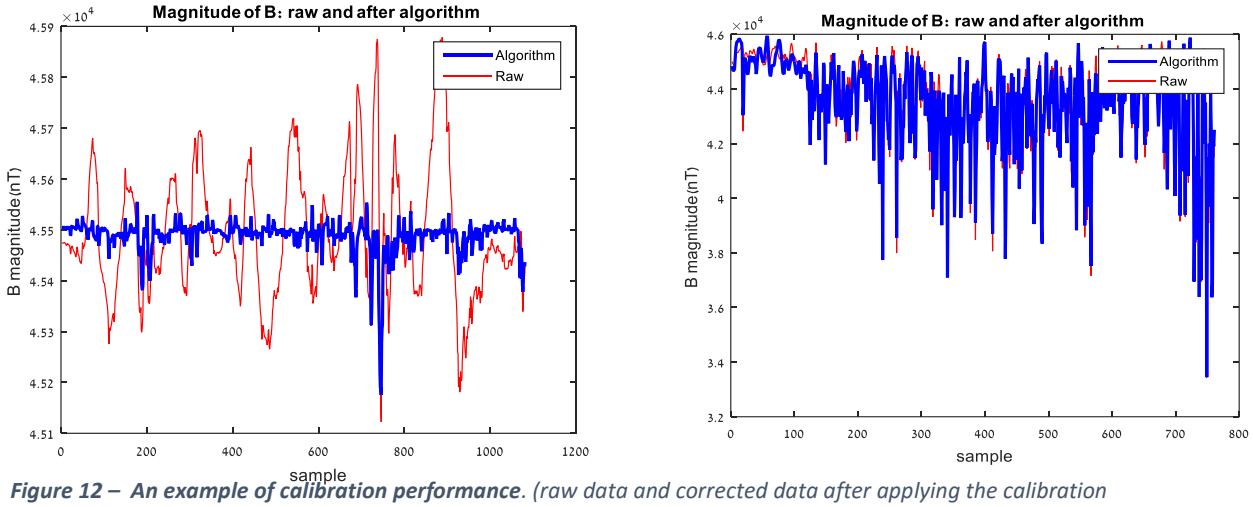

Figure 12 – An example of calibration performance*. (raw data and corrected data after applying the calibration algorithm) for slow rotation (left) and fast rotation (right).*

Width of averaging window

Different widths of averaging window were tested to improve the corrected magnetic magnitude. A wider widow seems to provide better results. The mean errors values for measurements which had different width of averaging window are shown in Table 4:

Width of moving averaging window	0.1 sec		0.25 sec		0.5 sec	
Error parameter	PTP	VAR	PTP	VAR	PTP	VAR
Value [nT]	14.25	5.28	13.96	5.24	13.67	5.22

***Table 4 – the effect of averaging window's width**, after applying the correction algorithm of each measurement independently (mean values)*

Sensor type, sampling frequency, and fitting Strategy

In the graphs below we present a summary of experimental results for different hardware and calibration configurations. All the results are for a system **without** an internal averaging, so all the averaging processing was done **after** applying the calibration algorithm. The parameters which were checked are magnitude max PTP error and the magnitude's variance. Note that the values in the graphs are the **mean** values, calculated from all the measurements relevant to the given hardware configuration. The results are shown in Figure 13 and Figure 14 :

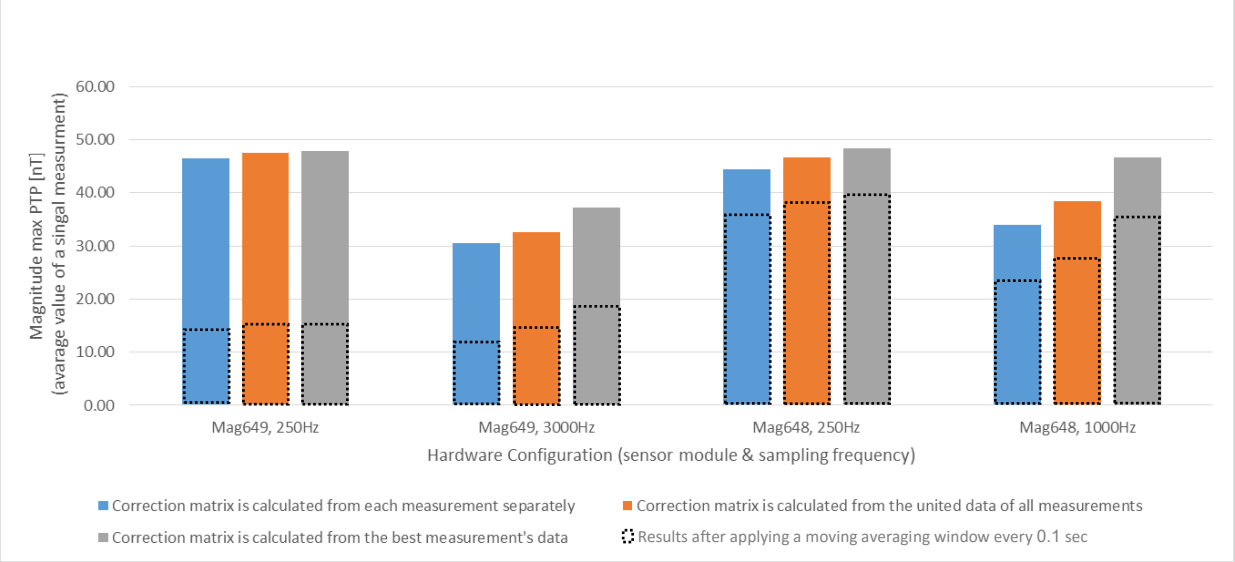

***Figure 13 – Mean values of magnitude max PTP for a single measurement** , with and without averaging (after the correction), as a function of hardware configuration and data used to calculate the correction matrix*

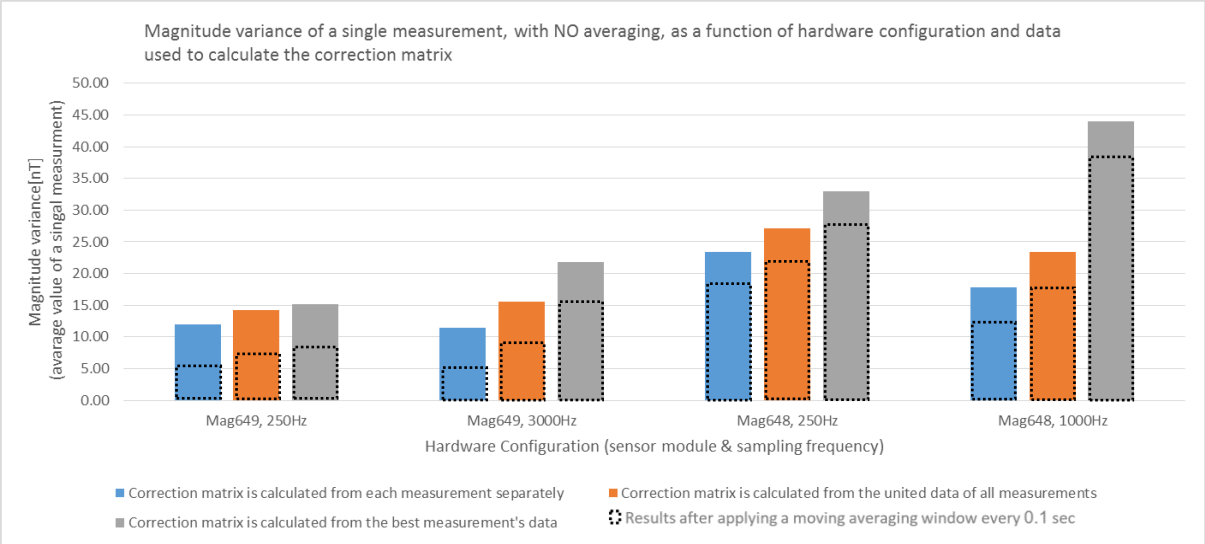

Figure 14 – Mean values of magnitude variance for single measurement *with and without averaging (after the correction), as a function of hardware configuration and data used to calculate the correction matrix*

Final configuration performance

Here we present the results for the system's final configuration (Mag 649 with sampling rate of 3000 Hz).

Calibration performance

The calibration performance of the final system configuration is shown in Table 5:

Raw data before correction		After applying the correction algorithm		After applying the correction algorithm + moving average window with 0.1 sec width	
PTP [nT]	Var [nT]	PTP [nT]	Var [nT]	PTP [nT]	Var [nT]
652	24,055	24	5	15	3

Table 5 – Final configuration performance*: magnitude max PTP and variance (mean values)*

A graphical demonstration of the input data we got for the calibration algorithm can be seen in Figure 15:

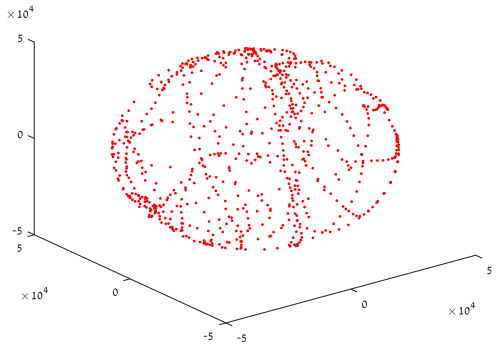

Figure 15- Points which were created during the sensor's spinning for the calibration process*. The axes are the x, y and z components of the magnetic field. As expected, the ellipsoid shape is observed.*

Figure 16 shows the magnetic magnitude before and after applying our calibration method:

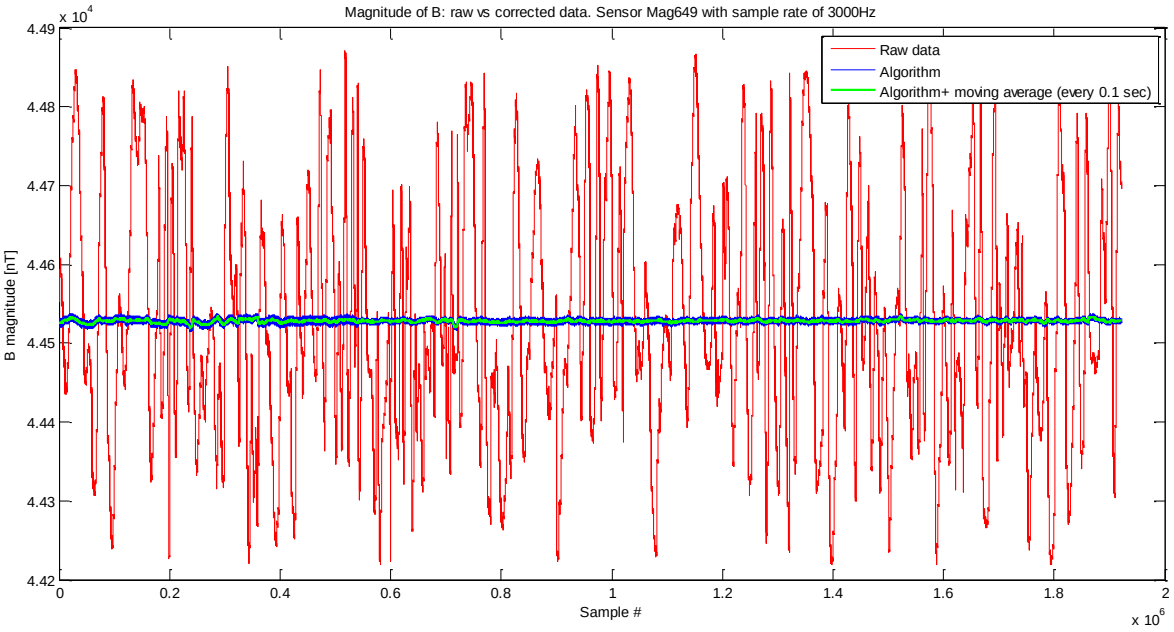

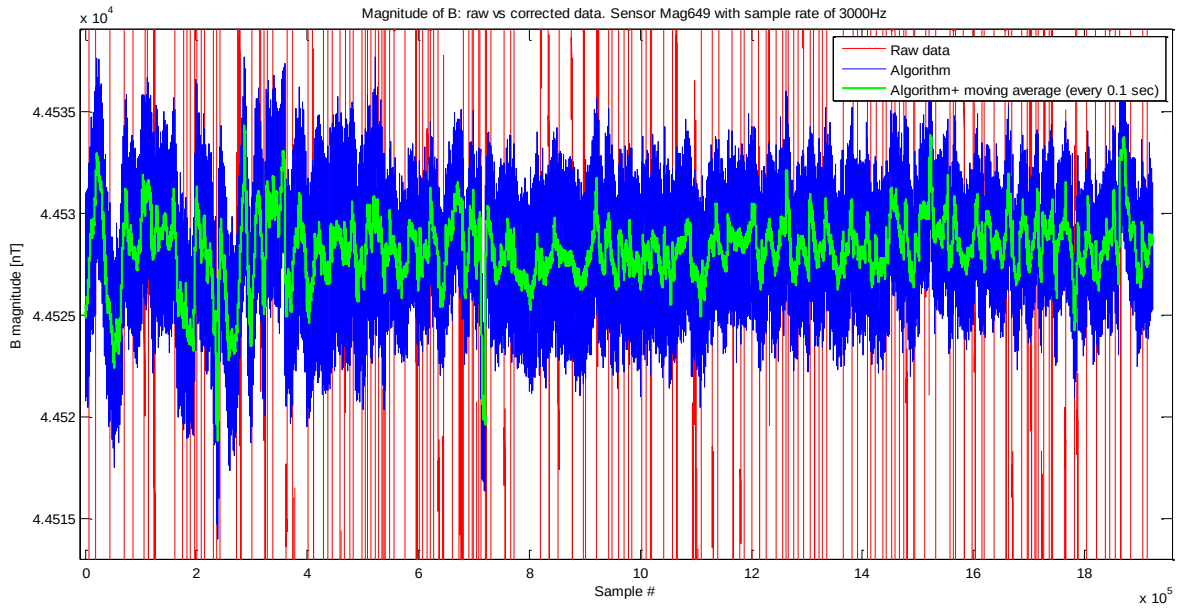

***Figure 16- Magnetic magnitude over 360 degrees sensor spin**, before and after applying the correction method, when using the system's final configuration. The lower graph in a magnification of the upper graph*

Mapping performance

An example of the performance of our mapping algorithm, when mapping an area which has a ferromagnetic element in the middle is shown in Figure 17:

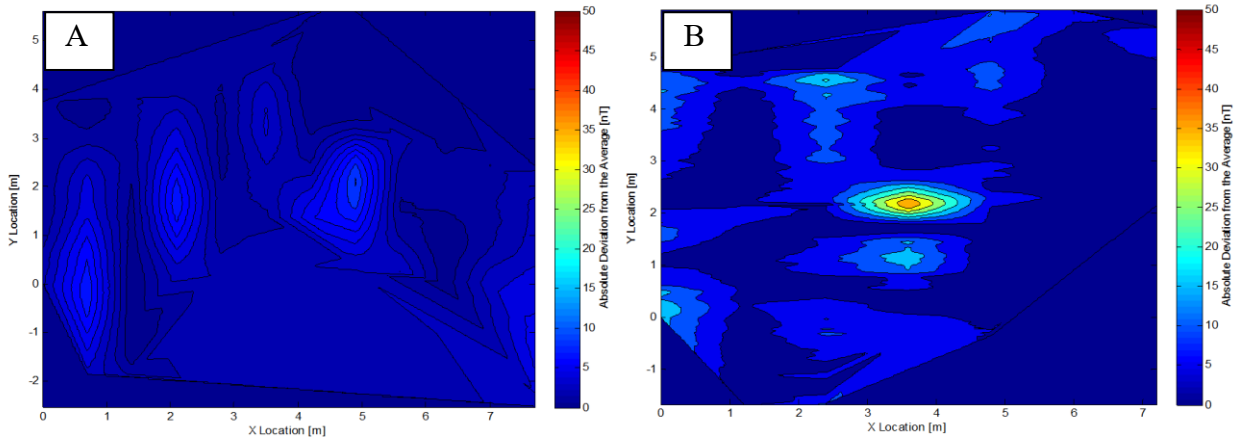

***Figure 17- A magnetic map on an area** without an ferromagnetic target (A) and with a ferromagnetic target (B)*

Discussion and Conclusions

The effect of controlled parameters on the system's performance

Averaging before applying the algorithm

As can be seen on Table 3, averaging data before applying the correction algorithm has a very negative influence on the system's performance. Hence, it is suggested to eliminate internal averaging processes.

Averaging after applying the algorithm

Table 6 summarizes the errors' differences between an averaged magnitude to non-averaged magnitude, after applying the same correction matrix, as can be seen in Figure 13 and Figure 14:

Configuration/ Max PTP	No averaging [nT[	With averaging [nT]	Difference (%)
Mag649, 250Hz	47	15	68
Mag649, 3000Hz	33	15	54
Mag648, 250Hz	47	38	18
Mag648, 1000Hz	40	29	27

Configuration/ Variance	No averaging [nT[	With averaging [nT]	Difference (%)
Mag649, 250Hz	14	7	49
Mag649, 3000Hz	16	10	38
Mag648, 250Hz	28	23	18
Mag648, 1000Hz	28	23	20

Table 6 – A Comparison of errors with and without averaging *for max PTP (left) and variance (right)*

It can be seen that when no averaging is applied, there is almost no difference between the max PTP performance of the Mag649 and the Mag648 with same sample rate. However, when applying the averaging, the Mag649 max PTP improves by 40-70%, while the Mag648 max PTP improves by only 20-30%. We assume this difference is due to much higher BW of the Mag649 compared to Mag648. Variance improves by 40-50% in the Mag649 and by ~20% in the Mag648.

Data source for calculating the correction matrix and offset

For all the hardware configurations that were checked, we found that the best data to minimize a given measurement's errors is the data of the measurement itself. Even though this conclusion may look trivial, it is not so obvious. One may think that if we take a longer united data from all the measurements or the data which yielded the result with the minimal error, it could improve the errors of a given measurement. Our experiments show that this is not the situation.

Considering how the algorithm operates can explain this conclusion: each measurement creates a slightly different ellipsoid, depending on the way the rotation was made and other random parameters. Thus, the best fit is made out of this "private case" of ellipsoid.

However, in real life we don't know the measurements that will be made by the system's operator in given conditions. Therefore, we have to find a way to minimize the mean error at all possible rotations, by calibrating the system in a finite amount of time. We have mentioned before 2 optional approaches to do it: choosing the calibration matrix of the best calibration experiment or creating a calibration matrix out of all the recorded data of a given hardware configuration. Table 7 shows the difference in magnitude errors between those two approaches (as can be seen in Figure 13 and Figure 14:):

	ptp		variance	
Configuration/ Data source for correction matrix	united data	best measurement	united data	best measurement
Mag649, 250Hz	10%	11%	42%	61%
Mag649, 3000Hz	22%	57%	77%	198%
Mag648, 250Hz	6%	10%	20%	51%
Mag648, 1000Hz	18%	51%	45%	211%

Table 7 – relative error (in %), compared to the calibration of each experiment separately

It can be seen that it is better to use the united data source rather than using the data of the best measurement. This inference makes sense since the united data contains more information about the sensor's possible orientations than the private case of the "best" experiment. Hence, the mean errors are expected to be lower.

Sensor module

Table 8 summarizes the differences between the 2 sensors modules by averaging the 2 sampling frequencies of each sensor:

Sensor/ Errors	PTP - no averaging [nT]	PTP - with averaging [nT]	Variance - no averaging [nT]	Variance - with averaging [nT]
Mag649	40	15	15	8
Mag648	43	33	25	20

Table 8 – the effect of the sensor's module *on a given measurement's errors. The shown numbers are the average of 2 frequencies measurements for each sensor's module*

From the above we can conclude that when it come to the magnitude's max PTP criterion, it seems that there is not much difference between and the Mag648 to the Mag649 when no averaging is performed. However, when averaging is performed, the PTP of the Mag649 is much better. As for the variance - there is a difference between the two modules (Mag649 is better), which becomes more notable when averaging is made.

Sampling rate

The influence of sampling rate is summarized in Table 9:

Configuration/ Variance	No averaging		With averaging every 0.1 sec	
	250Hz	1000Hz(648)/ 3000Hz(649)	250Hz	1000Hz(648)/ 3000Hz(649)
Mag649	47nT(PTP) 14nT(Var)	33nT(PTP) 16nT(Var)	17nT(PTP) 10nT(Var)	15nT(PTP) 8nT(Var)
Mag648	47nT(PTP) 27nT(Var)	38nT(PTP) 23nT(Var)	38nT(PTP) 22nT(Var)	28nT(PTP) 18nT(Var)

***Table 9 – the effect of the sample frequency**, when calibrating with the united data*

Looking at this table, we can see that higher sampling frequency has a positive effect on reducing the errors for both models.

A summation of effects

Table 10 summarizes some of the dependencies in the final system:

	Mag648		Mag649	
Magnitude's error parameter	Max PTP	Variance	Max PTP	Variance
Relative error for using "united data" calibration compared to the calibration of each experiment separately	6% (250Hz) to 18% (1000Hz)	20% (250Hz) to 45% (1000Hz)	10% (250Hz) to 22% (3000Hz)	42% (250Hz) to 77% (3000Hz)
Errors when calibrating with "united data" from several measurements WITHOUT Averaging	47 nT (250Hz) to 38 nT (1000Hz)	27 nT (250Hz) to 23 nT (1000Hz)	47 nT (250Hz) to 33 nT (3000Hz)	14 nT (250Hz) to 15 nT (3000Hz)
Averaging improvement (windows width = 0.1 sec)	20%	40%-50%	40-50%	20%-30%

***Table 10 – Summery of the influence of some parameters** on the system's performance*

Recommended system configuration and performance

The system configuration which gives the best performance according to our analysis is shown in Table 11:

System Specification	
Sensor module	Bartington Mag-649
Internal averaging (before applying the correction algorithm)	No
Hardware sampling rate	50KHz
Software sampling rate	3KHz
Calibration Method	
Calibration data source	United data of many measurements
Speed of spinning	Slow (~0.1 Hz)
Correction algorithm	Ellipsoid fit by RMS
Moving average window width	0.1 sec (10 Hz)

Table 11 – Final configuration Specification

A system with the written specifications, which is calibrated using the described calibration method, is expected to provide the following performance:

Error parameter	Value [nT]
Magnitude Max PTP	15
Magnitude Variance	3

Table 12 – Final configuration performance

Conclusions

The first stage of this work was the problem's definition. We developed a full physical model which was used to simulate several optional system configurations. Based on the simulation's conclusions, we built a fully functional system. Then, we conducted several field experiments in order to validate the simulation and to choose the optimal hardware and software configurations. Finally, we demonstrated a low- cost and simple system which performs a magnetic mapping with good resolution.

The main goals of the project were achieved. The experiments' results show the capability of using our calibration method for mapping purposes. The calibrated system has much better error rates, compared to a fluxgate sensor without the calibration. In addition, we found a suitable hardware configuration and modeled the effect of relevant parameters on the final system performance.

Moreover, the mapping algorithm which we developed has shown very good results in the field tests. Hence, it is now possible to achieve magnetic mapping capabilities by using a low cost fluxgate sensor, instead on using an expensive scalar magnetometer.

Further Work

Further work should consider the development of the following topics:

- Real time data – This work introduced a way to process magnetic data **after** it was collected. Future systems should improve this issue to enable real time data flow. This can be done by using a microprocessor which is connected directly to the sensor. The microprocessor can implement the calibration algorithm.
- Built in magnetic field generator – In this project we relied on a manual sensor's spinning to gather data at different sensor's orientations. The same result can be achieved by installing a small Helmholtz coil nearby the magnetic sensor. By changing the direction of the induced magnetic field during time, while maintaining its strength, it may be possible to gather calibration information without the need of physically spinning the sensor.
- Combining a few sensors together – Future work can reduce the measured errors by combining some magnetic sensors together. By comparing and averaging the magnetic data from several sources, it may be possible to improve the magnetic magnitude's PTP and variance errors[36].
- Testing another sensor model – Bartington's Mag-03 fluxgate sensor may have better performance compared to Mag 649 which we used in this project. It has a lower orthogonality error and a higher 3 -dB bandwidth. Based on our conclusions, those 2 parameters have an effect on the final performance. Therefore, it is recommended to test this sensor model.

Appendix 1 –Specifications of sensors

Here are the specifications of the sensors which were used during this project (Bartington Mag 648 and Mag 649):

Performance	
Number of axes	Three (Right Hand XYZ co-ordinate system)
Polarity	+ve non-inverting output when pointing North
Measuring range	±60µT or ±100µT
Bandwidth at-3dB: Mag648 Mag649	>30Hz >1kHz
Measurement noise floor: low noise standard noise	≤10pTrms/√Hz at 1Hz >10 to ≤20pTrms/√Hz at 1Hz
Scaling	50mV/µT (60µT) or 30mV/µT (100µT)
Start-up time	150ms
Warm-up time	15mins
Offset error	±100nT in zero field
Scaling error	±0.5% at DC
Temperature coefficient of offset error	1nT/°C
Temperature coefficient of scale factor	100ppm/°C
Orthogonality error	Less than 1° error between axes
Linearity error	0.0033% (least squares fit)
Frequency response (<5% deviation from DC): Mag648 Mag649	DC to 5Hz DC to 100Hz
Hysteresis	<2nT at 1 x full scale (when powered)
Excitation breakthrough: Mag648 Mag649	<10mV pk-pk at 4kHz <10mV pk-pk at 8kHz
MTBF	~21 years per MIL-217F-2(GB)

Environmental	
Operating temperature range	-40°C to +70°C
Storage temperature range	-40°C to +85°C
Environmental protection: Mag648/649 Mag648-MX & FL/Mag649-MX & FL Mag648S/Mag649S	 IP67 enclosure IP67; connector none IP68 (2000m depth)

Appendix 2 – Simulation results

The simulation tool we created helped us define the parameters of the final system configuration. Here we present some simulation results in order to demonstrate the iterative process which has been made.

All the simulations below were done while considering the effects which are described in the "Method for finding the best hardware configuration" section in the methods chapter. The calibration time for all the simulations which are presented here is 60 seconds and the sampling rate is 250Hz. Table 13 presents the effect of 2 parameters. The first one is the sensor's low pass bandwidth, and the second one is the effect of the internal averaging mechanism (every 5 samples). One can see that the simulation predicts the effect of changing those parameters.

	Raw PTP [nT]		Calibrated PTP [nT]	
Bandwidth of the sensor's LP filter (-3dB)	With internal averaging	Without internal averaging	With internal averaging	Without internal averaging
5Hz	2949	2570	2134	1556
30Hz	1319	1230	170	48
250Hz	1215	1187	54	7

Table 13 – an example of simulation results

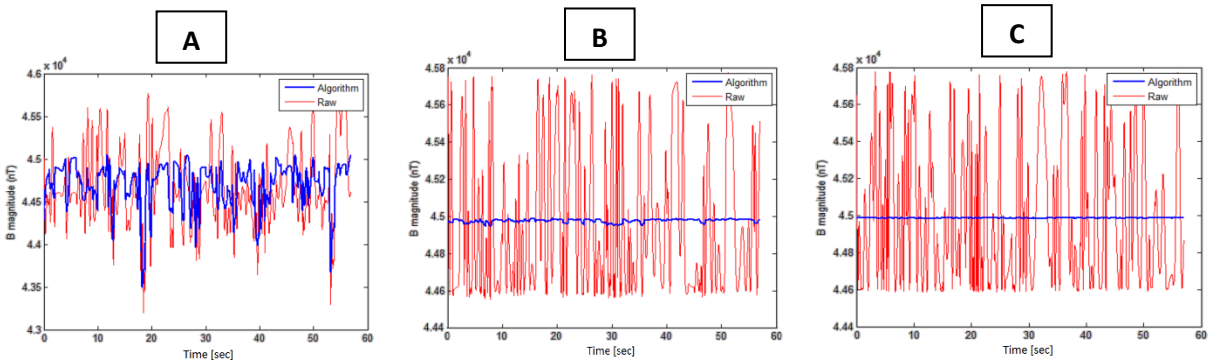

Graph 1 – Simulation results for the effect of changing the sensor's low pass filter BW (A=5Hz, B=30Hz, C=250Hz), for a system without internal averaging.

Acknowledgments

We would like to thank our instructor, Dr. Eyal Weiss, for his guidance, good advice, support and inspiration during this project. We have learned so much from you, and we are grateful for that. In addition, we would like to thank all the Soreq nuclear research center employees who helped us when we needed.

Finally, we would like to thank Noam Meyuhas and Yossi Kabessa from the Hebrew university for their good feedback throughout the last year.

References

[1] Cullity, Bernard Dennis, and Chad D. Graham. *Introduction to magnetic materials*. John Wiley & Sons, 2011.

[2] Bernold, L., Lashminarayan Venkatesan, and Sushil Suvarna. "A multi-sensory approach to 3-D mapping of underground utilities." *NIST SPECIAL PUBLICATION SP* (2003): 525-530.

[3] Sharma, Atul Prakash, and B. D. Tripathi. "Magnetic mapping of fly-ash pollution and heavy metals from soil samples around a point source in a dry tropical environment." *Environmental Monitoring and Assessment* 138.1-3 (2008): 31-39.

[4] Crew, Peter. "Magnetic mapping and dating of prehistoric and medieval iron-working sites in Northwest Wales." *Archaeological Prospection* 9.3 (2002): 163-182.

[5] Safizadeh, M. S., and M. Hasanian. "Gas pipeline corrosion mapping using pulsed eddy current technique." *International Journal of Advanced Design and Manufacturing Technology* 5.1 (2011): 11.

[6] Weiss, Eyal, et al. "High resolution marine magnetic survey of shallow water littoral area." *Sensors* 7.9 (2007): 1697-1712.

[7] "Magnetic Sensors and Magnetometers", P. Ripka, Artech, (2001)

[8] Lenz, James, and S. Edelstein. "Magnetic sensors and their applications." *IEEE Sensors journal* 6.3 (2006): 631-649.

[9] Wołszyn, Mirosław. "Locating and identifying ferromagnetic objects." *International Journal of Applied Electromagnetics and Mechanics* 39.1-4 (2012): 175-182.

[10] http://www.rmsinst.com/products/magnetometers/G823A.pdf

[11] http://quarrycrushing.gq/600tph/3570.html

[12] http://www.gmw.com/magnetic_measurements/Bartington/Mag-03_Pricing.html#Mag-03

[13] Primdahl, Fritz. "The fluxgate magnetometer." *Journal of Physics E: Scientific Instruments* 12.4 (1979): 241.

[14] Merayo, José MG, et al. "The orthogonalization of magnetic systems." *Sensors and Actuators A: Physical* 89.3 (2001): 185-196.

[15] Ripka, Pavel. "Advances in fluxgate sensors." *Sensors and Actuators A: Physical* 106.1 (2003): 8-14.

[16] Merayo, José MG, et al. "Scalar calibration of vector magnetometers." *Measurement science and* technology 11.2 (2000): 120.

[17] Marklund, G.T., Blomberg, L.G., Persson, S., 2001. Astrid-2, an advanced microsatellite for auroral research. Ann. Geophys. 19,
589–592

[18] Crassidis, John L., Kok-Lam Lai, and Richard R. Harman. "Real-time attitude-independent three-axis magnetometer calibration." *Journal of Guidance, Control, and Dynamics* 28.1 (2005): 115-120.

[19] Munschy, Marc, et al. "Magnetic mapping for the detection and characterization of UXO: Use of multi-sensor fluxgate 3-axis magnetometers and methods of interpretation." Journal of Applied Geophysics 61.3 (2007): 168-183.

[20] Merayo, José MG, et al. "The orthogonalization of magnetic systems." *Sensors and Actuators A: Physical* 89.3 (2001): 185-196.

[21] Auster, H. U., et al. "Calibration of flux-gate magnetometers using relative motion." *Measurement Science and Technology* 13.7 (2002): 1124-1131.
[22] Vasconcelos, J. F., et al. "A geometric approach to strapdown magnetometer calibration in sensor frame." *IFAC Proceedings Volumes* 41.1 (2008): 172-177.
[23] Ozyagcilar, Talat. "Calibrating an ecompass in the presence of hard and soft-iron interference." *Freescale Semiconductor Ltd* (2012).
[24] Claus, Brian, and Ralf Bachmayer. "A Parameterized Geometric Magnetic Field Calibration Method for Vehicles with Moving Masses with Applications to Underwater Gliders." *Journal of Field Robotics* (2016).
[25] Zhang, Xiaoming, and Lizhen Gao. "A novel auto-calibration method of the vector magnetometer." *Electronic Measurement & Instruments, 2009. ICEMI'09. 9th International Conference on*. IEEE, 2009.
[26] Feng, Wenguang, et al. "A calibration method of three-axis magnetic sensor based on ellipsoid fitting." *J. Inf. Comput. Sci* 10.6 (2013): 1551-1558.
[27] Pang, Hongfeng, et al. "A new calibration method of three axis magnetometer with nonlinearity suppression." *IEEE Transactions on Magnetics* 49.9 (2013): 5011-5015.
[28] Ackoff, Russell L. "Towards a system of systems concepts." *Management science* 17.11 (1971): 661-671.
[29] "Least-squares Fitting of a Three-dimensional Ellipsoid to Noisy Data." Ams Applied Mathematical Sciences (2014): n. pag. Web.
[30] Petrov, Yuri. "Ellipsoid Fit," MATLAB Central File Exchange, 2009.
[31] Zitzewitz, Paul & Neff, Robert. Physics. New York: Glencoe/McGraw-Hill, 1995.
[32] http://www.mathworks.com/help/signal/ug/iir-filter-design.html?requestedDomain=www.mathworks.com
[33] Korepanov, V., and R. Berkman. "Fluxgate magnetometer noise: theoretic and experimental study Measurements for a Sustainable Future." *Proc. 3rd Biennial Conf. MSA99 (Sydney, Australia)*. 1999.
[34] http://www.mathworks.com/help/matlab/ref/linspace.html
[35] "Ellipsoid_fit2magnetic_data." *GitHub*. Ozan AKTA, https://github.com/gzwsc2007/GroundStation/blob/master/software/ellipsoid_fit2magnetic_data.m
[36] Pang, Hongfeng, et al. "Calibration of a fluxgate magnetometer array and its application in magnetic object localization." *Measurement Science and Technology* 24.7 (2013): 075102.